Active Vibration Control (AVC) with Piezoelectric Actuators

Jonas Reiser

Physik Instrumente (PI) SE & Co. KG, Karlsruhe, Germany

j.reiser@pi.de

Abstract

High-precision mechatronic systems are increasingly influenced by external vibrations rather than intrinsic performance. The stiffness of the mounts strongly affects the sensitivity to disturbances. Soft mounts reduce the impact of indirect floor disturbances but increase sensitivity to direct forces, while ultra-hard mounts offer high position stability yet amplifying indirect floor vibrations. Passive solutions cannot address both effects simultaneously. Active vibration control using feedback damping and feedforward approaches can overcome these limitations. This work investigates AVC for ultra-hard, piezoelectric-based mounts using a real-time hardware-in-the-loop test setup. Performance is evaluated using power spectrum density and cumulative power spectrum metrics for position, velocity, and acceleration of the sensitive equipment in a frequency range from 0.2 Hz up to 2000 Hz. With online controller optimization up to 99.5 % vibration attenuation is achieved. The results are currently extended to a six-degree-of-freedom piezo hexapod system enabling multi-axes AVC.

Active Vibration Control, Vibration Damping and Isolation, Cumulative Power Spectrum, Feedforward and Feedback Control, Hardware-in-the-loop, Piezoelectric Actuators, DIRECT Algorithm, Ultra-hard Piezo Mount

1. Introduction

Ever-challenging requirements for position accuracy, stability and resolution in high-precision mechatronic systems can no longer be fulfilled by only improving the system's intrinsic performance. External disturbances, especially vibrations, increasingly limit the achievable performance. Since vibration isolation depends strongly on the mounting between sensitive equipment and the surrounding structure, mount stiffness is a key design parameter. Soft mounts reduce transmissibility and are beneficial for rejecting indirect disturbances, but they increase sensitivity to direct force disturbances. In contrast, ultra-hard mounts provide excellent stability and low sensitivity to direct disturbances but are more susceptible to indirect ones. Passive solutions cannot efficiently address both effects at the same time. Active vibration control (AVC) offers a way to overcome this trade-off. Feedback control is used to damp resonance modes of the mounting system, while feedforward control aims to suppress indirect disturbances before they enter the sensitive equipment. Although AVC is established for less stiff hard mounts, its application to ultra-hard mount systems based on piezoelectric actuators has not been investigated in detail [1, 2].

In this work, different AVC approaches are implemented on a real-time hardware-in-the-loop (HIL) setup with a single-axis piezoelectric test system that is shown in the Figure 1.

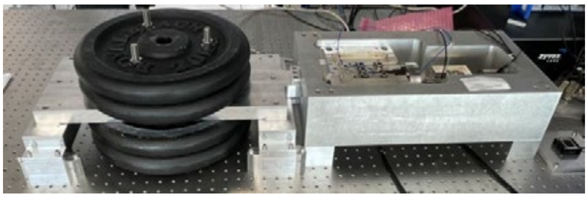

Figure 1: Single-axis piezo AVC test setup.

Both direct and indirect disturbances are applied to evaluate active damping and active isolation under controlled conditions. Performance is assessed in the time and frequency domains using the power spectral density (PSD) and cumulative power spectrum (CPS) of the measured position, velocity, and acceleration on the sensitive equipment. Open-loop (OL) and closed-loop (CL) results are compared. An online optimization algorithm is developed to minimize the CL CPS within a predefined frequency range by automatically tuning the controller parameters for the current disturbance conditions.

The results are summarized in CPS performance heatmaps, enabling a systematic comparison of the different AVC approaches. With optimized parameters, CPS reductions of up to 99.5 % in the range from 0.2 Hz to 2000 Hz are achieved relative to OL operation. Finally, the findings are transferred to a six-degree-of-freedom (6-DOF) piezo hexapod system, including the design of a dedicated 6-DOF excitation platform for introducing indirect disturbances.

2. AVC Test Setup

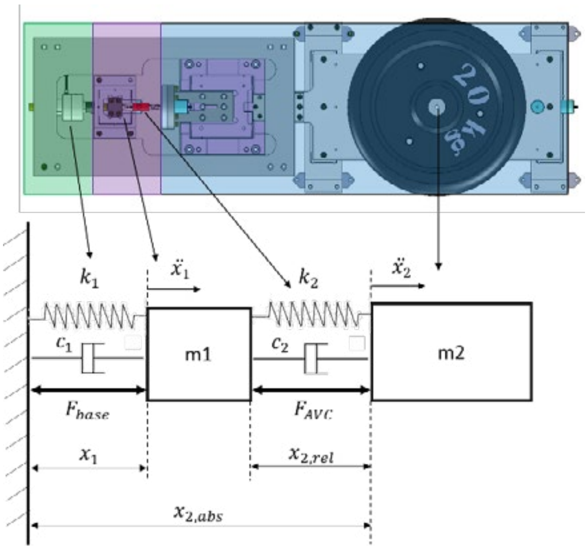

Figure 2: Single-axis AVC test setup (top) and mechanical schematic drawing (bottom).

A single-axis test setup (see Figure 2) is developed to evaluate the performance and applicability of several feedback and feedforward control approaches for an ultra-hard piezoelectric mount. The mount is realized using a low-voltage (LV) piezo actuator (P-843.20, Physik Instrumente (PI) SE & Co. KG) that connects the sensitive equipment, modeled by mass m_2, to a "virtual floor" represented by mass m_1. This virtual floor corresponds to the base of the LV actuator and is subjected to indirect disturbances generated by a high-voltage (HV) piezo actuator (P-235.1S, Physik Instrumente (PI) SE & Co. KG), which couples the real fixed ground to the virtual floor m_1.

Direct disturbances acting on the sensitive equipment m_2 are introduced via a second, virtual axis of the LV piezo actuator, which operates independently of the damping axis. Indirect disturbances acting on m_1 are defined using the vibration criteria by Colin G. Gordon, which specify acceptable floor vibration levels for different applications, ranging from VC-A (optical microscopy) to VC-G (extremely quiet research environments). In this work, the VC-C criterion, described as a good standard for lithography and inspection equipment in the semiconductor industry, is used [2, 3, 4].

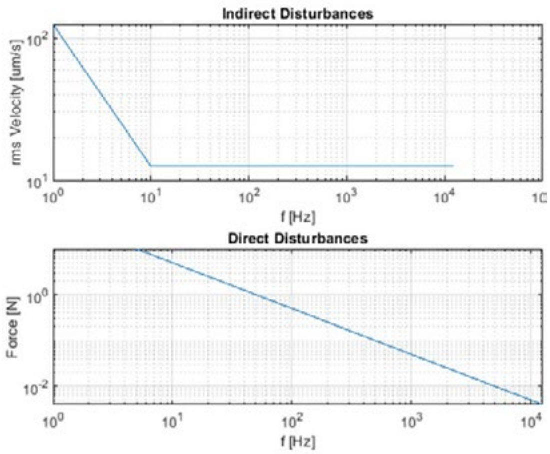

Figure 3: Excitation spectra for indirect (top) and direct (bottom) disturbances.

Direct disturbances on m_2 are represented by a force spectrum shown in Figure 3 together with the indirect disturbance spectrum. Both spectra are converted into voltage/time signals and are used as target inputs for the corresponding piezo actuators.

The test setup is equipped with multiple sensors. Accelerometers (393B05, PCB Piezotronics GmbH) and capacitive position sensors (D-510.021, D-050.01A + D-050.02A, Physik Instrumente (PI) SE & Co. KG) are used to measure the accelerations and positions of both masses m_1 and m_2. The velocities $\dot{x}_1$ and $\dot{x}_2$ are obtained by applying a velocity bandpass filter (VBP) with corner frequencies ω_{low} and ω_{high} of 1 Hz and 2000 Hz. The VBP filter's transfer function is given by:

$$K_{VBP} = g_{VBP} \cdot K_{INT} \cdot K_{BP} = \frac{g_{VBP}}{s + \omega_{low}} \cdot \frac{\omega_{high}}{s + \omega_{high}} \quad (1)$$

2.1 AVC Strategies under Test

To evaluate the performance and applicability of AVC strategies, commonly used for soft and hard mounts, on an ultra-hard piezoelectric mount, several approaches are implemented and systematically compared. All strategies are realized on a Speedgoat real-time target machine (Speedgoat GmbH), which communicates with a digital piezo controller (E-712, Physik Instrumente (PI) SE & Co. KG) via a serial peripheral interface (SPI).

Table 1 provides an overview of the AVC approaches investigated in this work, categorized by measured feedback and feedforward signals.

Table 1: List of all AVC approaches under test.

Position-based	Acceleration-based	Control
Absolute Positive Position Feedback (aPPF)	Negative Acceleration Feedback (NAF)	Feedback
Relative Positive Position Feedback (rPPF)	Direct Velocity Feedback (DVF)	
Absolute Negative Position Feedback (aNPF)	Velocity Bandpass Filter (VBP)	
Relative Negative Position Feedback (rNPF)	Special Velocity Bandpass Filter (VBP E712)	
Position Feedforward in combination with VBP (FF Pos)		Feedforward + Feedback

The block-diagram representation of a general AVC system, including feedback and feedforward, is shown in the following figure. The transfer functions P_T and P_C represent the transmissibility and the compliance of the passive structure, respectively. Transfer function K_{FB} corresponds to the feedback controller and K_{FF} to the feedforward controller dynamic.

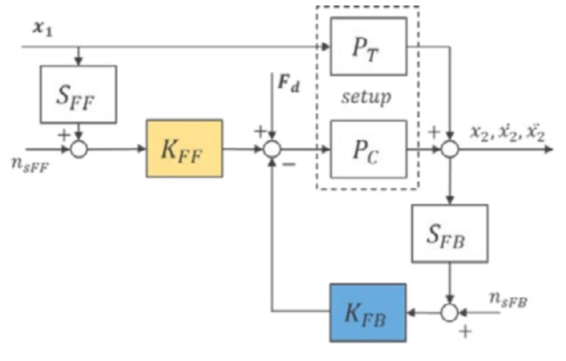

Figure 4: Block-diagram representation of a general AVC system, including feedback and feedforward controllers.

2.2 AVC Performance Metrics

The objective of vibration control is to minimize motion of the sensitive mass m_2. Performance of the AVC approaches is evaluated using time- and frequency-domain metrics. In the time domain, root mean square (RMS) and peak-to-peak (PTP) values of x_2, $\dot{x}_2$ and $\ddot{x}_2$ are compared with and without AVC. In the frequency domain, transmissibility and compliance curves as well as resonance peak attenuation are assessed.

The primary metric is the CPS, obtained by integrating the PSD within a given frequency range from f_1 to f_2:

$$CPS(f) = \int_{f_1}^{f_2} PSD(v)\, dv \tag{2}$$

The CPS describes the total error across frequencies, with the final value at f_2 equaling the squared RMS [2]. In this work, CPS is evaluated from f_1 = 0.2 Hz up to f_2 = 2000 Hz. The goal is to minimize this value, targeting a CL/OL CPS ratio < 1.0 (100 %).

2.3 CPS Optimization Algorithm

To automatically optimize controller parameters for specific use cases, an algorithm minimizing the CPS value is developed in this work. Figure 5 shows the flowchart of this algorithm.

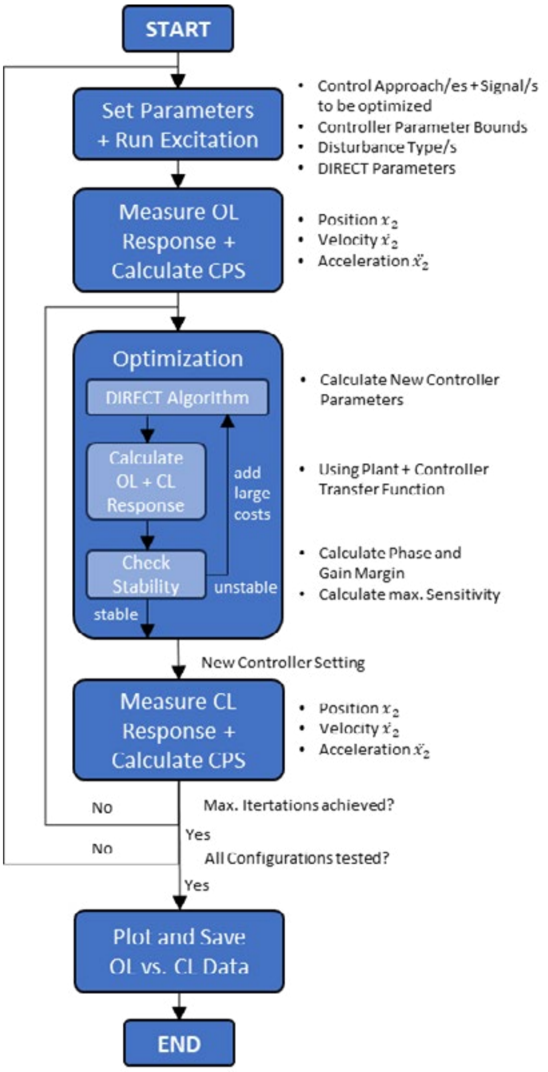

Figure 5: Flowchart representation of the developed CPS minimization algorithm.

The algorithm minimizes the CPS of position x_2, velocity $\dot{x}_2$, acceleration $\ddot{x}_2$, or a weighted combination thereof, depending on application priorities. The minimization uses the DIRECT optimization algorithm [5]. Based on identified plant and controller transfer functions, it predicts OL gain and CL response within parameter bounds, while enforcing stability (gain/phase margins) and robustness criteria (maximum sensitivity S). Large “cost” is added for unstable solutions to ensure convergence to the global minimum which must fulfill a stable, robust controller setting. Optimal parameters are verified online on the real setup, with corresponding CPS values computed.

3. AVC Test Results

Final minimal CPS values for all combinations of disturbance type, control approach, and optimized signal(s) are summarized in CPS performance heatmaps, enabling direct comparisons.

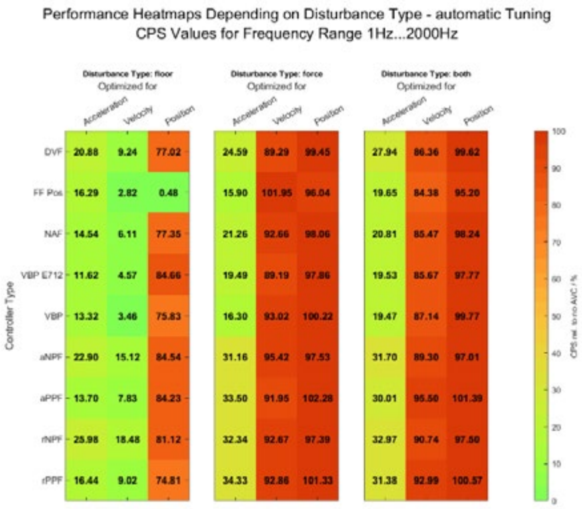

Figure 6: Performance heatmaps showing the online minimized CPS values for the three different disturbance types and all AVC approaches under test.

Nearly all approaches improve performance compared to OL operation. Acceleration- (or velocity-) based AVC outperforms position-based methods. The best result is achieved with position feedforward (FF Pos) combined with VBP feedback under pure floor disturbances: position CPS is reduced to 0.48 % of OL operation, with velocity CPS also minimal among all approaches.

For floor disturbances only, the CPS order is velocity < acceleration < position. This arises from the triangular OL gain interacting with the disturbance spectrum shape. Indirect floor disturbances have largest impact at low frequencies but stay also constant in a wide frequency range (see Figure 3). The corresponding acceleration spectrum corresponds to a counterclockwise rotation of the velocity spectrum, increasing high frequency impact (excitation of higher modes). Position spectrum represents a clockwise rotation compared to the velocity spectrum, amplifying the low frequency disturbances but also attenuating the high frequency impact. Thus, the velocity spectrum provides the optimal trade-off, maximizing damping around the resonance frequency without low/high-frequency excitation.

For force or combined disturbances, the CPS order shifts to acceleration < velocity < position, due to the strongly descending force spectrum. Force dominates floor disturbance, with position spectrum attenuating most at resonance, while acceleration still enables effective damping without overexciting higher modes.

In Figure 7, exemplary transmissibility and compliance plots compare all approaches using online-optimized parameters. FF Pos shifts transmissibility downward across a wide range up to or even beyond resonance, achieving good isolation of mass m_2. Since FF Pos uses only x_1, its compliance matches VBP feedback approach (green and yellow compliance curve on top of each other). All feedback approaches showing varying damping performances.

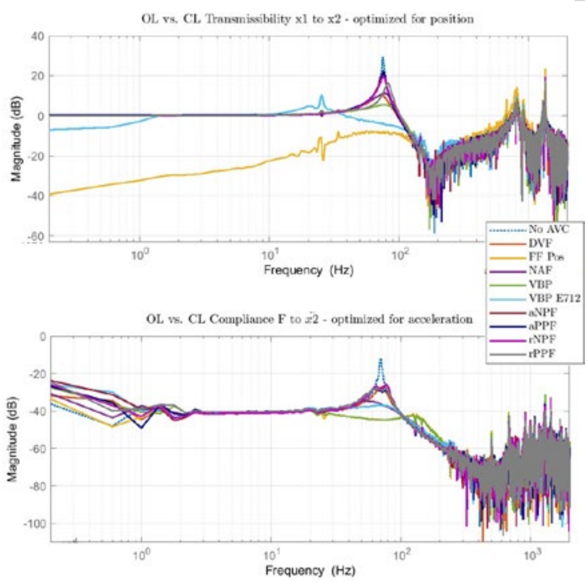

Figure 7: Exemplary transmissibility (top) and compliance (bottom) plots for all AVC approaches with online-optimized controller settings – Floor (top) and force (bottom) disturbances only, optimized for minimal position (top) and acceleration (bottom) CPS.

4. Summary

This work evaluates multiple AVC approaches for various disturbance types on a single-axis piezoelectric test setup. A DIRECT-based online algorithm minimizes CPS of position x_2, velocity $\dot{x}_2$ and acceleration $\ddot{x}_2$ in the range of 0.2 Hz to 2000 Hz, with results summarized in performance heatmaps enabling a comparison of all approaches depending on the use case. There is no dedicated AVC approach that excels universally. VBP feedback shows best overall performance. For dominant floor vibrations, VBP combined with position feedforward achieves best isolation behavior. Transmissibility shifts downward (by -40 dB) up to or even beyond resonance frequency of the setup, reducing position CPS to 0.49 % of OL operation. Acceleration-/velocity-based approaches outperform position-based methods. CPS rankings depend on disturbance spectra in combination with OL gain: floor disturbances leading to following CPS order: velocity < acceleration < position, force-dominant cases shift CPS order to acceleration < velocity < position.

5. Future Work

Future work will focus on adaptive online CPS minimization to update controller parameters when disturbance conditions change over time. In addition, feedforward control for direct force disturbances shall be investigated to reduce compliance over a wider frequency range. Finally, the results from the single-axis setup will be transferred to a 6-DOF system. For this purpose, a HV piezo excitation platform (see Figure 8) and a dedicated LV piezo AVC hexapod are being commissioned to enable indirect and direct disturbances in six axes (Figure 9). FEM analyses indicate that a 40 kg payload ensures sufficient resonance separation between both stages, which is essential for stable multi-axis operation.

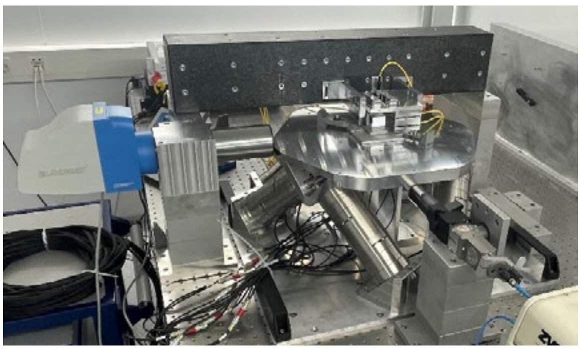

Figure 8: 6-DOF HV piezo excitation platform during multi-axes calibration.

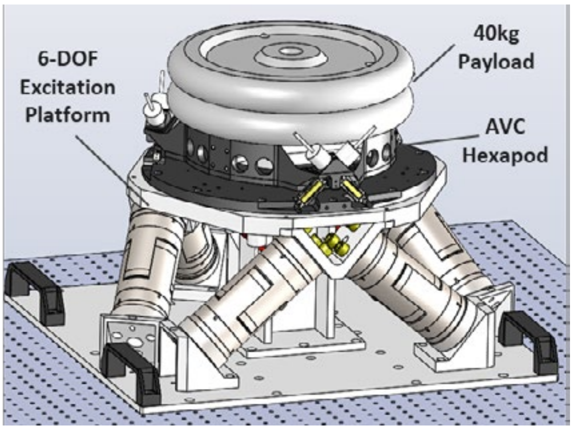

Figure 9: Multi-axes test setup showing the LV piezo AVC hexapod with 40 kg payload on top of the 6-DOF HV piezo excitation platform.

References

[1] Kaczmarek M B. “Frequency-domain design for non-conventional Active Vibration Control”, Ph.D. dissertation, Precision and Microsystems Engineering (PME), Delft University of Technology (TU Delft), 2025.

[2] Neele M J. “Ultra Hard Mount Active Vibration Control”, M.Sc. thesis, Faculty of Mechanical Engineering, Delft University of Technology (TU Delft), 2024.

[3] Gordon C G. “Generic vibration criteria for vibration-sensitive equipment”. In: *Optomechanical Engineering and Vibration Control.* vol. 3786. SPIE. 1999, pp. 22–33.

[4] Goht C J and Caugheys T K. “On the stability problem caused by finite actuator dynamics in the collocated control of large space structures”. In: *Taylor and Francis,* 41 (3 1985), pp. 787–802. ISSN: 1366-5820.

[5] Finkel D E (2003). “DIRECT Optimization Algorithm User Guide (Version 4.0)”, Technical Report CRSC-TR03-11, Center for Research in Scientific Computation, NC State University, 2003.